ACS OMEGA

Open Access

http://pubs.acs.org/journal/acsodf

Article

Tolerance of Perovskite Solar Cells to Electrostatic Discharge in Martian Dust Activities

Dong Liu,* Xianyuan Jiang, Zhongchen Wu,* Xianyang Sun, and Ying-Bo Lu

Cite This: *ACS Omega* 2024, 9, 25215−25222

Read Online

ACCESS | Metrics & More | Article Recommendations | Supporting Information

ABSTRACT: In exploring the viability of perovskite solar cells (PSCs) for Mars missions, our study first delved into their temperature endurance in conditions mimicking the Martian climate, revealing remarkable thermal stability within the temperature range of 173−303 K. We then pioneered the examination of PSC resilience to electrostatic discharge (ESD), a critical factor given the frequent Martian dust activities. In a custom-built Martian simulation chamber, we discovered that ESD exposure dramatically reduced the power conversion efficiency of these devices by more than half (55.4%) in just 90 s. This groundbreaking research not only advances our understanding of the potential of PSCs for Mars exploration but also opens new avenues for optimizing solar technology in extreme environments.

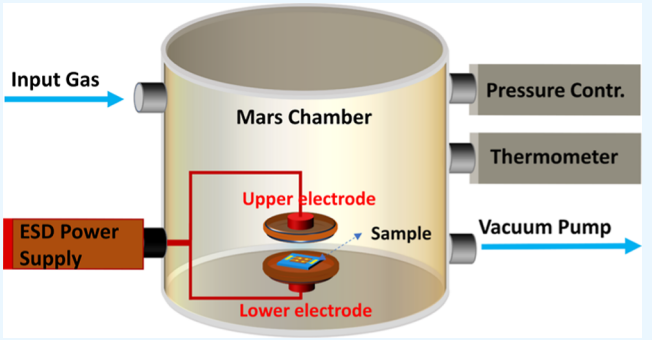

1. INTRODUCTION

Solar power is an inexhaustible source of energy for deep space exploration missions, especially for the Martian and Lunar. Currently, high-efficiency space photovoltaic technologies such as silicon, GaAs, InP, and III−V multijunction solar cells with lifetimes exceeding 10 years in low-earth orbit are widely used in spacecraft and satellites.[1] With the continuous development of space applications, such as space stations and Moon/Mars surface bases, the next generation of space exploration projects will require increasingly more power. Therefore, there is a high demand for new photovoltaic technologies in the upcoming space competition.

Organic−inorganic hybrid perovskites show great potential for highly efficient thin-film solar cells due to panchromatic light absorption, long carrier lifetime, low exciton binding energy, high defect tolerance, and low-temperature solution-based fabrication method.[2−6] The waterless and oxygen-free conditions of space are more conducive to the stable operation of perovskite solar cells (PSCs). PSCs are inexpensive to manufacture and have a higher power-to-weight ratio compared to existing III−V multijunction solar cells.[7] Additionally, the previous studies demonstrate significant advantages of PSCs in lightweight and tolerance under high-energy particle irradiations. Kang et al. have successfully fabricated ultralight and flexible PSCs with the orthogonal silver nanowire transparent electrodes, which demonstrated a remarkable power-per-weight ratio of 29.4 W g^{-1}.[8] Lang et al. reported that the triple-cation PSCs maintain 95% of its initial efficiency after proton irradiation with an energy of 68 MeV and a total dose of 10^{12} cm^{-2}.[9] Noteworthy, several groups have already tracked the behavior of PSCs in real space environment to promote their space applications. In 2018, Manca et al. conducted a high-altitude balloon flight experiment that reached an altitude of 32 km to track the performance of PSCs and to observe the evolution of maximum power point over time and temperature.[10] In 2019, Zhu et al. sent their mixed-cation PSCs into near space through a high-altitude balloon at an altitude of 35 km to track the stability of mixed-cation PSCs.[11] The device absorber sustained 95.19% of its original power conversion efficiency (PCE) during the test. In 2020, Buschbaum et al. reported the launch of PSCs on a suborbital rocket flight, tracking device current−voltage characteristics in variable illumination states.[12] These studies suggest that perovskite photovoltaic materials have great potential for use in space applications.

There will be substantial power requirements for a future Mars surface base, and there is little doubt that solar cells will play an important role. However, there remains a lack of electrostatic discharge (ESD) tolerance investigations of PSCs under the dust activities based on a simulated Martian surface environment, which could be helpful in evaluating the application potential of PSCs on Mars. Dust is pervasive in the Martian environment. In massive global dust storms, the fast Martian winds at low pressure can carry vast amounts of

Received: March 25, 2024
Revised: May 2, 2024
Accepted: May 17, 2024
Published: May 23, 2024

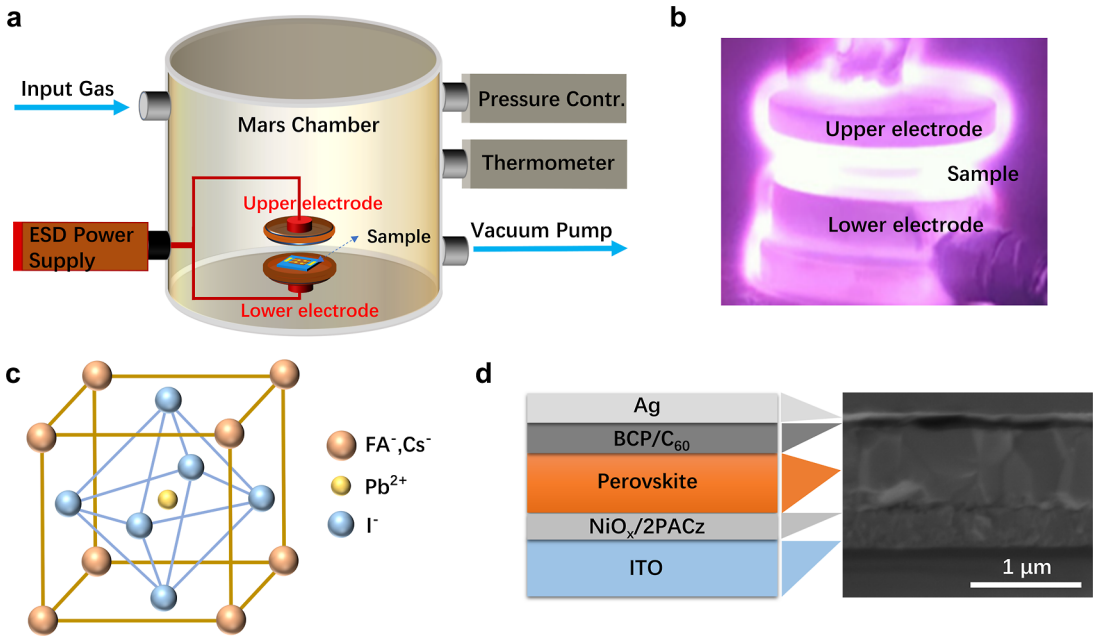

Figure 1. (a) Schematic diagram of the MEC for the ESD experiments. Upper and lower electrodes used in the ESD experiment, with a PSC on the lower electrode. (b) Photograph of the ESD-generated plasma between the upper and lower electrodes. (c) Crystal structure of the $Cs_{0.03}FA_{0.97}PbI_3$ perovskite material. (d) Sketch and cross-sectional SEM of the investigated inverted PSCs.

dust and generate ESD phenomena,[13,14] resulting in occlusion or abrasion of solar cells. Sand and dust particles on Mars surfaces can become electrically charged through friction, resulting in smaller grains carrying negative charges and larger grains carrying positive charges of similar composition.[15−17] During convective aeolian processes, lighter grains with a negative charge are lifted upward while heavier grains with a positive charge remain closer to the surface, resulting in the generation of an active electric field (E-field).[18−20] The likelihood of ESD on Mars is higher due to its thin atmosphere, which has a significantly lower breakdown E-field threshold (BEFT) compared to Earth's BEFT.[21−24] Therefore, investigating the performance evolution of PSCs under ESD in Martian dust activities is crucial for future base station construction on the Mars surface.

Herein, we fabricated the $Cs_{0.03}FA_{0.97}PbI_3$-based PSCs with a sandwich structure consist of ITO/NiO_x/[2-(9*H*-carbazol-9-yl)ethyl]phosphonic acid (2PACz)/perovskite/C_{60}/bathocuproine (BCP)/Ag. First, the temperature tolerance of PSCs in simulated Martian temperatures was investigated. The PSCs exhibited sufficient thermal stability against temperature changes between 173 and 303 K. Subsequently, we constructed a Martian chamber capable of simulating ESD in Martian dust activities and conducted the first-ever investigation on the ESD tolerance of PSCs. We demonstrate a significant decline of 55.4% in the PCE of the PSCs within an exposure time of 90 s to ESD. These investigations indicate that ESD in Martian dust activities is an enormous challenge for the future application of PSCs on Mars.

2. EXPERIMENTAL SECTION

2.1. Materials. Lead iodide (PbI_2) (Xi'an Polymer Light Technology, 99.99%), cesium iodide (CsI) (Sigma-Aldrich, 99.999%), FAI (Xi'an Polymer Light Technology), *N*,*N*-dimethylformamide (DMF) (Sigma-Aldrich, anhydrous, 99.8%), dimethyl sulfoxide (DMSO) (Sigma-Aldrich, anhydrous, 99.9%), anisole (Sigma-Aldrich, J&K Seal, Super Dry, water ≤20 ppm, 99.7%), isopropanol (IPA) (Sigma-Aldrich, anhydrous, 99.5%), NiO*x* (Xi'an e-Light New Material), C_{60} (Xi'an Polymer Light Technology), [2-(9*H*-carbazol-9-yl)-ethyl]phosphonic acid (2PACz) (TCI, >98.0%), and bathocuproine (BCP) (TCI, purified by sublimation, 99.0%) were all used as received without further purification.

2.2. Device Fabrication. The prepatterned ITO substrates were cleaned by an ultrasonic instrument by sequentially washing with a DI water bath with 2% Triton X-100 v/v, DI water, and IPA for 30 min each. The blow-dried ITO substrates were cleaned by UV−ozone treatment for 20 min, followed by spin coating the NiO_x ink (20 mg mL^{-1} in IPA: DI = 1:3 v/v) at 3000 rpm for 30 s and then annealed at 100 °C for 10 min. A 0.5 mM 2PACz solution in ethanol was spin-coated on a NiO_x substrate at 3000 rpm for 30 s and then annealed at 100 °C for 10 min. The precursor was spin coated at 1500 and 6000 rpm for 15 and 25 s, respectively. During the second stage, 150 μL anisole was dropped onto the surface at the last 10 s, and the substrate was annealed at 100 °C for 10 min. C_{60} (23 nm) and BCP (8 nm) layers were successively formed by thermally evaporating. Finally, approximately 100 nm Ag electrodes were deposited on top of the BCP layer by thermal evaporation under a high vacuum. The PSCs were encapsulated by a cover glass with UV glue (Loctite 3106).

2.3. Device and Film Characterization. A Keithley 2400 source unit was employed to obtain *J*−*V* curves under simulated AM1.5 solar illumination at 100 mW cm^{-2} (1 sun). For the *J*−*V* curve measurement, the active area of all the devices was masked using a metal mask with an area of 0.04 cm^2. The calibration of light was enabled by a KG-5 Si diode with a solar simulator (Enli Tech, Taiwan). The devices are measured in reverse scan (1.15−0 V, step 0.01 V) and forward scan (0−1.15 V, step 0.01 V) with a delay time of 30 ms at room temperature.

2.4. Mars Chamber and EDS Experiments. In this study, one Mars environment chamber (MEC) was built at Shandong University, Weihai. The ESD normal glow discharge (NGD)

https://doi.org/10.1021/acsomega.4c02887
ACS Omega 2024, 9, 25215−25222

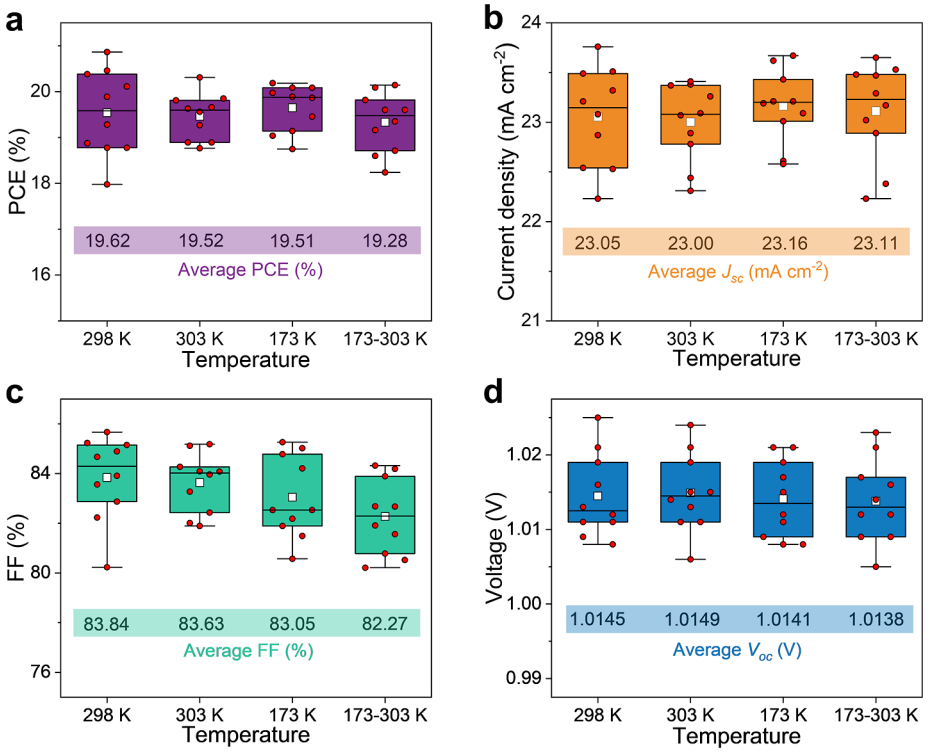

Figure 2. Performance of solar cells for various temperature experiments. The statistics for (a) PCE, (b) J_{sc}, (c) FF, and (d) V_{oc} were derived from the $J-V$ curves of the solar cells tested under various temperature experiments.

experiment of PSCs was conducted in the MEC to investigate the tolerance of PSCs under the ESD induced by Mars dust activities. A schematic diagram of the MEC and peripheral function units is shown in Figure 1a. The MEC has the capability to regulate Mars-relative environmental parameters (gas pressure, gas components, and temperature) and can also be attached to multiple in situ spectral measurement units. For accurate and reliable measurement and control of gas pressure (from 0.1 to 1000 Pa), the MEC integrates a pressure sensor, an electronic mass flow meter, a gas pressure controller, and an oil-free vacuum pump. In addition, a customized four-channel gas mixer with four electronic gas flowmeters was utilized for in situ mixing of CO_2, N_2, Ar, and O_2 during pumping. The composition of the gases could be easily adjusted. The temperature of the MEC was regulated by a customized heating and cooling stage, which was installed inside the MEC and connected to a temperature controller and a liquid nitrogen pump by electronic and gas feedthroughs. The controllable temperature (−123 to 473 K) covered the temperature range of the Martian surface with good uniformity and stability (±0.5 K). The ESD-NGD setup involved two copper electrodes, each with a diameter of 35 mm, placed within the MEC. These electrodes were positioned at a fixed distance of 6.0 mm from each other. We used an alternating current power (220 V, 50 kHz) plasma generator connected to a touch voltage regulator that was directly connected to the discharge electrodes in the MEC. All experiments were carried out at room temperature.

3. RESULTS AND DISCUSSION

Although the Martian atmosphere does not meet the general requirements for generating lightning, it is possible to generate electrical discharges in the event of strong surface winds during a large dust storm on Mars. The measurement of negative potential gradients on Earth has revealed values reaching several thousand volts per meter during dust storms with sufficiently strong winds.[25,26] Owing to a lower pressure in the Martian atmosphere, the required voltage for electrical breakdown is lower than on Earth.[27−29] The numerical simulation of the electrostatic field in Mars dust devils has been studied by many workers using different experimental technique models. Farrell and co-worker found that large vertical E-fields (20 kV m^{-1}) can develop in the dust devil on Mars using an electrodynamic model.[14] Conti and Williams investigated the breakdown potential gradient under varying CO_2 densities, revealing a maximum of only 20 kV m^{-1} in the Martian atmosphere with CO_2 densities of 2×10^{17} cm^{-1}.[30] Eden and Vonnegut investigated the breakdown potential gradient of dust in a CO_2 atmosphere at low pressure (10 mbar), showing only 5 kV m^{-1}.[31] On the basis of the known breakdown potential gradient of Martian dust and past laboratory experiments, the tolerance of PSCs in the ESD of Martian dust devils was examined by E-fields of 20 kV m^{-1}.

The Martian surface environment is a complex system characterized by intricate climatic conditions, significant dust accumulation, and the presence of intense cosmic radiation, all of which have the potential to hinder the power generation capability of PSCs.[32−34] To streamline the simulation process and concentrate on investigating the effects of ESD and temperature on the PSCs, this study solely simulated ESD and temperature variations specific to Mars, without considering other environmental factors.[35] A schematic diagram of the MEC and peripheral function units is illustrated in Figure 1a. The configuration of the MEC is shown in Figure S1. The ESD experiment of PSCs was conducted in the MEC to investigate the tolerance of PSCs under ESD induced by Mars dust activities. A photograph of the ESD-generated plasma between the upper and lower electrodes is shown in Figure 1b.

https://doi.org/10.1021/acsomega.4c02887
ACS Omega 2024, 9, 25215−25222

Considering the balance between stability and efficiency, we fabricated inverted PSCs based on a sandwich structure consisting of ITO/NiO_x/2PACz/perovskite/C_{60}/BCP/Ag.[36] The chemical formula of the perovskite is confirmed to be $Cs_{0.03}FA_{0.97}PbI_3$. The schematic of the perovskite crystal, the PSC structure, and the cross-sectional scanning electron microscopy (SEM) are shown in Figure 1c,d, respectively. The C_{60} and NiO_x serve as an electron-transporting layer (ETL) and a hole-transporting layer (HTL), respectively. The perovskite layer (thickness, ≈650 nm) of various cation/anion compositions was prepared by spin-coating precursors on the HTL. The C_{60} and BCP layers were successively formed by thermally evaporating. The Ag layer (thickness of ≈100 nm) was thermally deposited on top of the ETL layer. PSCs were encapsulated using UV glue with a cover glass without any impact on device performance. Figure S2 shows the typical current density versus voltage (J−V) curve of the PSCs under AM 1.5 illumination, which yields a champion PCE of 21.02% with a short-circuit current density (J_{sc}) of 23.36 mA cm^{-2}, an open-circuit voltage (V_{oc}) of 1.05 V, and a fill factor (FF) of 85.72%.

Temperature plays a key role in the operation of PSCs, as they largely determine the carrier transport characteristics (responsible for V_{oc}) and the magnitude of the series resistance (responsible for the FF). Therefore, prior to conducting ESD experiments, the thermal stability of PSCs was assessed. Subsequently, PSCs were packed in aluminum-covered evacuated container. A variety of orbiters and landed missions have obtained measurements of ground and near-surface air temperatures (temperature extremes: 175−298 K) on Mars.[7,37,38] Then, we designed two experiments to study the effect of Mars temperature on the PSCs. The first experiment, PSCs were exposed to temperatures of 303 and 173 K, corresponding to the highest and lowest temperatures of the Mars surface, respectively. In the second experiment, the solar cells were exposed to a cyclic temperature change from 173 to 303 K, simulating the diurnal temperature changes of the Martian environment. As a result, for up to 100 h of experimental testing, all encapsulated PSCs mostly maintained performance without losing J_{sc} and V_{oc} at 173 and 303 K, as well as under cyclic temperature changes, as shown in Figure 2 and Tables S1−S4. The test result can be ascribed to the protective natureof the packaging and the perovskite material at low temperatures, similar to some previous studies.[39,40] Moreover, this implies that the temperature conditions prevailing on the Martian surface do not inflict any detrimental impact on PSCs, thereby highlighting the significant potential of PSCs as prospective solar cell candidates for Mars.

The perovskite film serves as the crucial light absorption layer, constituting the pivotal component in PSCs.[6] It effectively harnesses solar radiation to generate excitons, subsequently facilitating the generation of electrons and holes. To explore the effect of ESD on the PSCs, we first characterized the perovskite film at different ESD times (from 0 to 90 s) due to its crucial role in PSCs. As shown in Figure 3a, the pristine perovskite film without ESD (0 s) exhibited a compact and homogeneous morphology. However, the surface of perovskite films exhibited the presence of pinholes and uneven shading subsequent to the ESD treatment, as shown in Figure 3b−d. The presence of pinholes at grain boundaries is evidently prominent and can be potentially attributed to the heightened susceptibility of grain boundary defects to ESD damage. Moreover, an increase in the ESD exposure time correlates with a progressive augmentation in the incidence of pinholes.

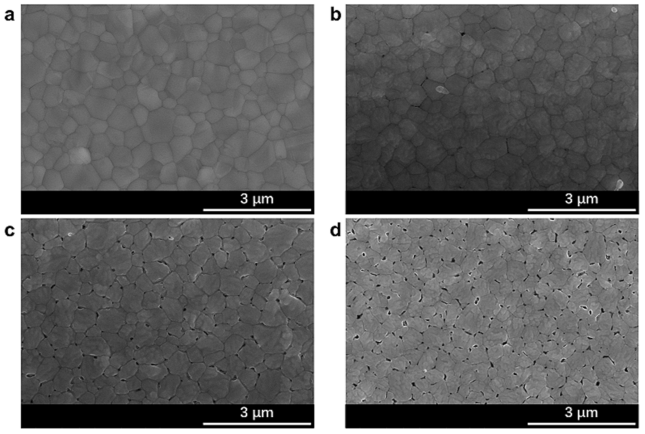

Figure 3. SEM images of perovskite films (a) without ESD and with ESD times of (b) 30, (c) 60, and (d) 90 s, respectively.

In order to better understand the effect of ESD on the crystal structure, we conducted X-ray powder diffraction (XRD) measurement for the perovskite films under various ESD times, as shown in Figure 4a. For the pristine perovskite films, the peaks at 13.92, 19.76, 24.26, and 28.08° were assigned to the (100), (110), (111), and (200) crystal planes of cubic phase (α-phase), respectively. Meanwhile, a diffraction peak of hexagonal phase (δ-phase) appears at 26.5°. The XRD peaks of perovskite films with ESD are observed to shift toward a higher diffraction angle compared to the pristine film, as depicted in Figure 4b−f. This phenomenon can be attributed to the crystal lattice distortion induced by ionic migration. Furthermore, after ESD treatment, a decreasing trend was evident in all α-phase peaks, excluding δ-phase peaks. This indicates that the crystal quality of the perovskite films was reduced, and the transition from α-phase to δ-phase was enhanced by the ESD treatment.

To simulate the operation of the devices under ESD conditions, we tested PSCs within various ESD time intervals ranging from 0 to 90 s. Each device was used only once to eliminate any potential cross-effects. Figure 5a shows images of solar cells under various ESD times. The color of packaging materials deepens, and the damage of unpacked silver electrodes intensifies with prolonged ESD time. The J−V curves under AM1.5G illumination for both the solar cells and the reference devices when exposed to different ESD durations are depicted in Figure 5b. Figure 5c−f depicts mean values of four sets consisting of ten devices each that were tested under 0, 30, 60, and 90 s ESD duration. The detailed data are summarized in Table S5−S8. The data demonstrate that the PCE, the J_{sc}, the FF, and the V_{oc} of PSCs are reduced with the ESD time accumulation. The J_{sc}, V_{oc}, FF, and PCE exhibit reductions of 33.3, 18.4, 18.5, and 55.4%, respectively, under both the ESD duration conditions of 0 and 90 s.

To investigate the effects of the ESD conditions on PSCs, we meticulously processed and analyzed the experimental data. As shown in Figure 6a, by fitting the correlation between V_{oc} and ESD times, it was observed that the rate of decrease in V_{oc} exhibited an accelerated trend. Based on the fitting curve of J_{sc} and ESD times, a linear decreasing trend was observed for J_{sc} without any abrupt decline, as shown in Figure 6b. Initially rapid, followed by gradual decline, characterized the relationship between FF and ESD times, as shown in Figure 6c. Similar

https://doi.org/10.1021/acsomega.4c02887
ACS Omega 2024, 9, 25215−25222

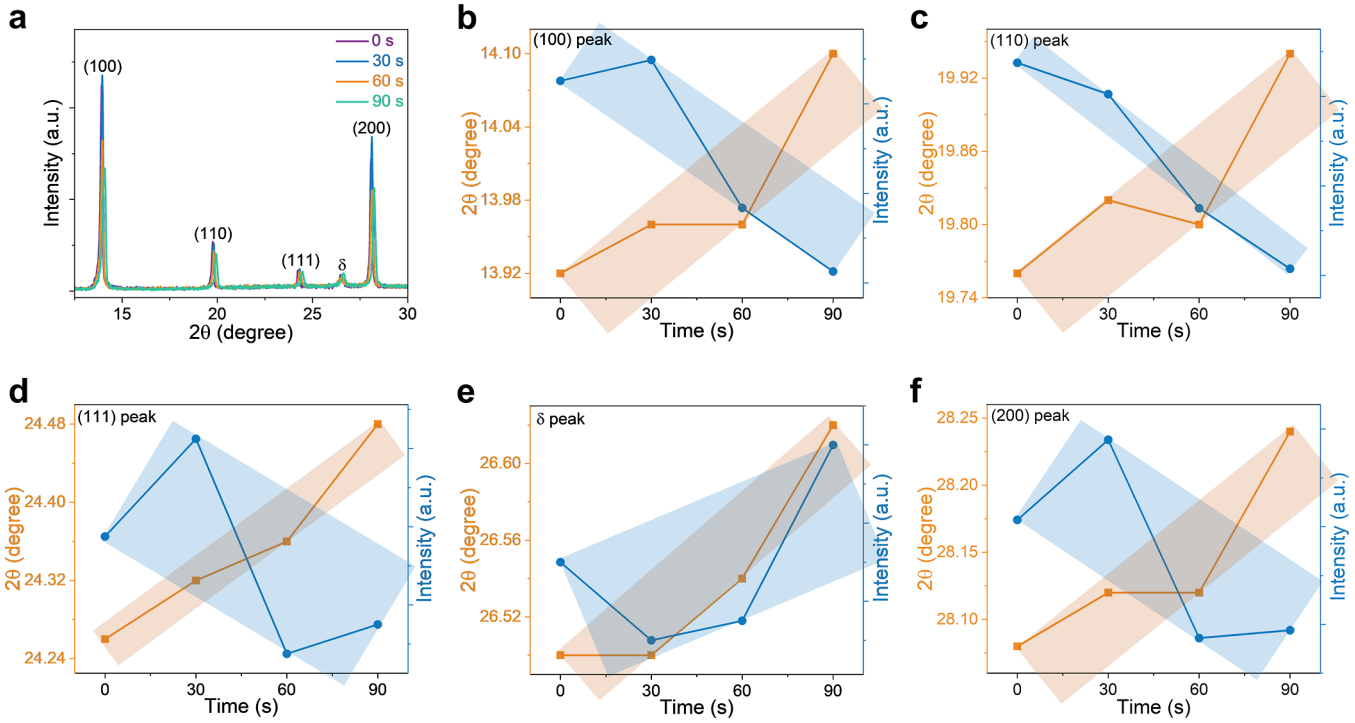

Figure 4. XRD characterization of perovskite films. (a) XRD patterns were recorded as a function of the ESD time ranging from 0 to 90 s for perovskite film. The XRD peak position and intensity were shown as a function of the ESD time for the (b) (100) peak, (c) (110) peak, (d) (111) peak, (e) δ peak, and (f) (200) peak.

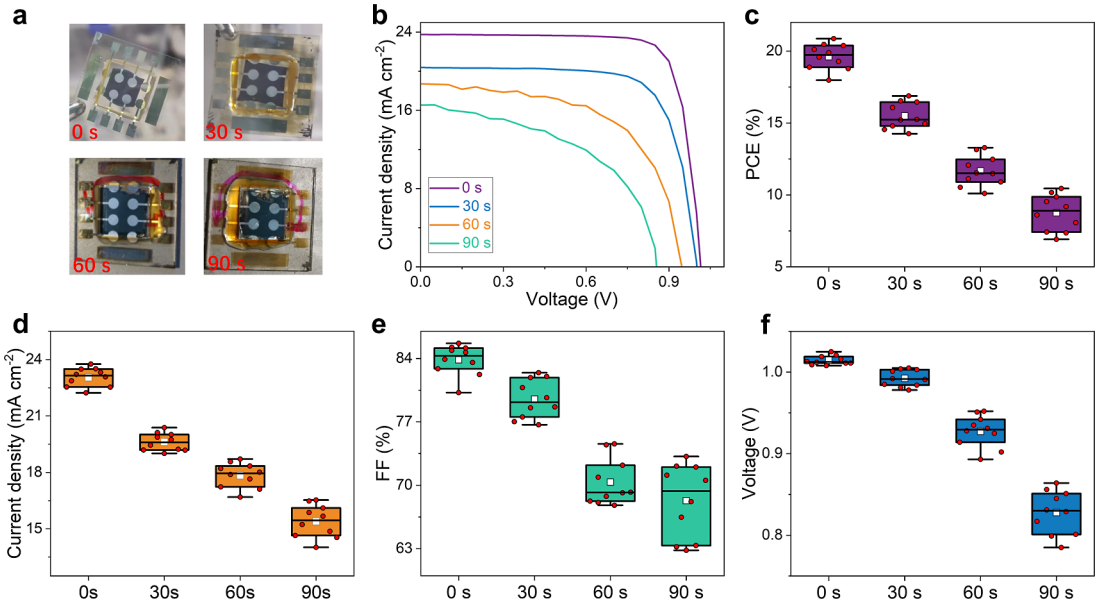

Figure 5. Performance of solar cells for the ESD experiments. (a) Images of solar cells under various ESD times. (b) $J-V$ curves under AM1.5G illumination at 1 sun intensity. The statistics for (c) PCE, (d) J_{sc}, (e) FF, and (f) V_{oc} were derived from the $J-V$ curves of the solar cells tested under various ESD times.

to the J_{sc}-ESD time curves, the PCE−ESD time curves also displayed a similar pattern due to the combined effects of opposing trends of the FF-ESD time and the V_{oc}-ESD time curves, as shown in Figure 6d. Furthermore, the standard deviation of the four parameters is calculated. It is found that as the ESD time increases, the standard deviation of the device parameters also increases, which indicates that ESD significantly affects the stability of the device performance. These findings highlight the enormous challenges posed by ESD in Martian dust activity, forcing us to think carefully about the future application of PSCs on Mars.

4. CONCLUSIONS

Our study evaluates the Martian suitability of $Cs_{0.03}FA_{0.97}PbI_3$-based PSCs with a structure of ITO/NiO_x/2PACz/perovskite/C_{60}/BCP/Ag. We confirmed their impressive thermal stability across Martian temperatures from 173 to 303 K. Through experiments in a custom-built Martian chamber simulating

https://doi.org/10.1021/acsomega.4c02887
ACS Omega 2024, 9, 25215−25222

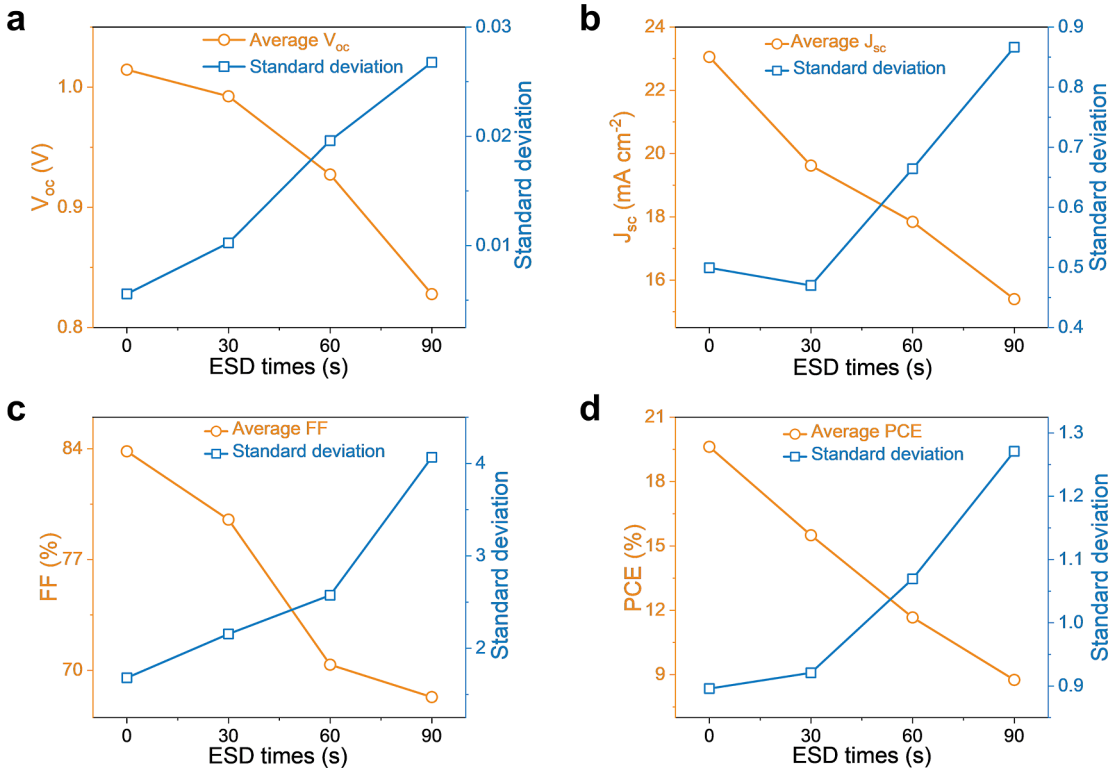

Figure 6. Both the average and standard deviation of (a) V_{oc}, (b) J_{sc}, (c) FF, and (d) PCE performance parameters for PSCs under different ESD times.

ESD from dust activities, we discovered a dramatic 55.4% drop in PCE after just 90 s of ESD exposure. This research underscores the potential of PSCs in Mars exploration while guiding future enhancements for solar cells under extreme conditions.

■ ASSOCIATED CONTENT

Supporting Information

The Supporting Information is available free of charge at https://pubs.acs.org/doi/10.1021/acsomega.4c02887.

Photograph of the MEC and ESD simulator, typical $J-V$ curve of the PSC with a champion PCE of 21.02% under AM 1.5 illumination, performance data for PSCs under various temperatures (173, 298, and 303 K, and the cyclic changes from 173 to 303 K), and performance data for PSCs under various ESD times (0, 30, 60, and 90 s) (PDF)

■ AUTHOR INFORMATION

Corresponding Authors

Dong Liu − *School of Space Science and Physics, Shandong University, Weihai 264209, China; Shandong Key Laboratory of Optical Astronomy and Solar-Terrestrial Environment, Institute of Space Sciences, Shandong University, Weihai 264209, China;* orcid.org/0009-0007-1901-4604; Email: shendongliu@126.com

Zhongchen Wu − *School of Space Science and Physics, Shandong University, Weihai 264209, China; Shandong Key Laboratory of Optical Astronomy and Solar-Terrestrial Environment, Institute of Space Sciences, Shandong University, Weihai 264209, China;* orcid.org/0000-0003-3199-4012; Email: z.c.wu@sdu.edu.cn

Authors

Xianyuan Jiang − *School of Physical Science and Technology, ShanghaiTech University, Shanghai 201210, China;* orcid.org/0000-0001-5966-0175

Xianyang Sun − *School of Space Science and Physics, Shandong University, Weihai 264209, China; Shandong Key Laboratory of Optical Astronomy and Solar-Terrestrial Environment, Institute of Space Sciences, Shandong University, Weihai 264209, China*

Ying-Bo Lu − *School of Space Science and Physics, Shandong University, Weihai 264209, China; Shandong Key Laboratory of Optical Astronomy and Solar-Terrestrial Environment, Institute of Space Sciences, Shandong University, Weihai 264209, China;* orcid.org/0000-0001-7799-8751

Complete contact information is available at: https://pubs.acs.org/10.1021/acsomega.4c02887

Notes

The authors declare no competing financial interest.

■ ACKNOWLEDGMENTS

We appreciate Dr. Zhou Wei of ShanghaiTech University for his experimental help. This work was supported by the Shandong Provincial Natural Science Foundation, China (no. ZR2020MA067) and the National Natural Science Foundation of China under Grant 11504202. This work was supported by the Physical-Chemical Materials Analytical and Testing Center of Shandong University, Weihai.

■ REFERENCES

(1) Verduci, R.; Romano, V.; Brunetti, G.; Yaghoobi Nia, N.; Di Carlo, A.; D'Angelo, G.; Ciminelli, C. Solar Energy in Space

Applications: Review and Technology Perspectives. *Adv. Energy Mater.* **2022**, *12*, 2200125.
(2) Liu, M.; Johnston, M. B.; Snaith, H. J. Efficient planar heterojunction perovskite solar cells by vapour deposition. *Nature* **2013**, *501*, 395−398.
(3) Liu, D.; Jiang, L.; Jiang, X.; Sun, X.; Zhang, G.; Lu, Y.-B.; Wang, Y.; Wu, Z.; Ling, Z. Interface-Tension-Assisted Temperature-Gradient Crystallization of High-Quality $MAPbBr_3$ Perovskite Single Crystals with Low Defect Densities. *ACS Appl. Mater. Interfaces* **2023**, *15*, 57846−57855.
(4) Dong, Q.; Fang, Y.; Shao, Y.; Mulligan, P.; Qiu, J.; Cao, L.; Huang, J. Electron-hole diffusion lengths > 175 μm in solution-grown $CH_3NH_3PbI_3$ single crystals. *Science* **2015**, *347*, 967−970.
(5) Wu, J.; Liu, D.; Lu, Y.-B.; Wu, Z.; Zhao, Y.; Dong, L.; Cong, W.-Y. Investigations on the Strong Light-Changed Photoluminescence Performance and the Crystalline Structure of $MAPbBr_1Cl_2$ Mixed Halide Perovskites. *J. Phys. Chem. C* **2023**, *127*, 23428−23435.
(6) Liu, D.; Zhou, W.; Tang, H.; Fu, P.; Ning, Z. Supersaturation controlled growth of $MAFAPbI_3$ perovskite film for high efficiency solar cells. *Sci. China Chem.* **2018**, *61*, 1278−1284.
(7) Ho-Baillie, A. W. Y.; Sullivan, H. G. J.; Bannerman, T. A.; Talathi, H. P.; Bing, J.; Tang, S.; Xu, A.; Bhattacharyya, D.; Cairns, I. H.; McKenzie, D. R. Deployment Opportunities for Space Photovoltaics and the Prospects for Perovskite Solar Cells. *Adv. Mater. Technol.* **2022**, *7*, 2101059.
(8) Kang, S.; Jeong, J.; Cho, S.; Yoon, Y. J.; Park, S.; Lim, S.; Kim, J. Y.; Ko, H. Ultrathin, lightweight and flexible perovskite solar cells with an excellent power-per-weight performance. *J. Mater. Chem. A* **2019**, *7*, 1107−1114.
(9) Lang, F.; Jost, M.; Bundesmann, J.; Denker, A.; Albrecht, S.; Landi, G.; Neitzert, H.-C.; Rappich, J.; Nickel, N. H. Efficient minority carrier detrapping mediating the radiation hardness of triple-cation perovskite solar cells under proton irradiation. *Energy Environ. Sci.* **2019**, *12*, 1634−1647.
(10) Cardinaletti, I.; Vangerven, T.; Nagels, S.; Cornelissen, R.; Schreurs, D.; Hruby, J.; Vodnik, J.; Devisscher, D.; Kesters, J.; D'Haen, J.; Franquet, A.; Spampinato, V.; Conard, T.; Maes, W.; Deferme, W.; Manca, J. V. Organic and perovskite solar cells for space applications. *Sol. Energy Mater. Sol. Cells* **2018**, *182*, 121−127.
(11) Tu, Y.; Xu, G.; Yang, X.; Zhang, Y.; Li, Z.; Su, R.; Luo, D.; Yang, W.; Miao, Y.; Cai, R.; Jiang, L.; Du, X.; Yang, Y.; Liu, Q.; Gao, Y.; Zhao, S.; Huang, W.; Gong, Q.; Zhu, R. Mixed-cation perovskite solar cells in space. *Sci. China Phys. Mech. Astron.* **2019**, *62*, 974221.
(12) Reb, L. K.; Böhmer, M.; Predeschly, B.; Grott, S.; Weindl, C. L.; Ivandekic, G. I.; Guo, R.; Dreißigacker, C.; Gernhäuser, R.; Meyer, A.; Müller-Buschbaum, P. Perovskite and Organic Solar Cells on a Rocket Flight. *Joule* **2020**, *4*, 1880−1892.
(13) Melnik, O.; Parrot, M. Electrostatic discharge in Martian dust storms. *J. Geophys. Res.* **1998**, *103*, 29107−29117.
(14) Farrell, W. M.; Delory, G. T.; Cummer, S. A.; Marshall, J. R. A simple electrodynamic model of a dust devil. *Geophys. Res. Lett.* **2003**, *30*, 2050.
(15) Kok, J. F.; Renno, N. O. Electrostatics in Wind-Blown Sand. *Phys. Rev. Lett.* **2008**, *100*, 014501.
(16) Forward, K. M.; Lacks, D. J.; Sankaran, R. M. Particle-size dependent bipolar charging of Martian regolith simulant. *Geophys. Res. Lett.* **2009**, *36*, L13201.
(17) Krauss, C. E.; Horányi, M.; Robertson, S. Experimental evidence for electrostatic discharging of dust near the surface of Mars. *New J. Phys.* **2003**, *5*, 70.1−70.9.
(18) Esposito, F.; Molinaro, R.; Popa, C. I.; Molfese, C.; Cozzolino, F.; Marty, L.; Taj-Eddine, K.; Di Achille, G.; Franzese, G.; Silvestro, S.; Ori, G. G. The role of the atmospheric electric field in the dust-lifting process. *Geophys. Res. Lett.* **2016**, *43*, 5501−5508.
(19) Farrell, W. M.; Smith, P. H.; Delory, G. T.; Hillard, G. B.; Marshall, J. R.; Catling, D.; Hecht, M.; Tratt, D. M.; Renno, N.; Desch, M. D.; Cummer, S. A.; Houser, J. G.; Johnson, B. Electric and magnetic signatures of dust devils from the 2000 - 2001 MATADOR desert tests. *J. Geophys. Res.* **2004**, *109*, No. E03004.
(20) Harrison, R. G.; Barth, E.; Esposito, F.; Merrison, J.; Montmessin, F.; Aplin, K. L.; Borlina, C.; Berthelier, J. J.; Déprez, G.; Farrell, W. M.; Houghton, I. M. P.; Renno, N. O.; Nicoll, K. A.; Tripathi, S. N.; Zimmerman, M. Applications of Electrified Dust and Dust Devil Electrodynamics to Martian Atmospheric Electricity. *Space Sci. Rev.* **2016**, *203*, 299−345.
(21) Rahman, M. M.; Cheng, W.; Samtaney, R. Generation and sustenance of electric fields in sandstorms. *Phys. Rev. Res.* **2021**, *3*, L012008.
(22) Farrell, W. M.; McLain, J. L.; Collier, M. R.; Keller, J. W.; Jackson, T. J.; Delory, G. T. Is the electron avalanche process in a martian dust devil self-quenching? *Icarus* **2015**, *254*, 333−337.
(23) Winn, W. P.; Schwede, G. W.; Moore, C. B. Measurements of Electric Fields in Thunderclouds. *J. Geophys. Res.* **1974**, *79*, 1761−1767.
(24) Zhai, Y.; Cummer, S. A.; Farrell, W. M. Quasi-electrostatic field analysis and simulation of Martian and terrestrial dust devils. *J. Geophys. Res.* **2006**, *111*, No. E06016.
(25) Stow, C. D. Dust Sand Storm Electrification. *Weather* **1969**, *24*, 134−144.
(26) Kamra, A. K. Measurements of the Electrical Properties of Dust Storms. *J. Geophys. Res.* **1972**, *77*, 5856−5869.
(27) Loeb, L. B. The Mechanisms of Stepped and Dart Leaders in Cloud-to Ground Lightning Strokes. *J. Geophys. Res.* **1966**, *71*, 4711−4721.
(28) Grard, R. Solar Photon Interaction with the Martian Surface and Related Electrical and Chemical Phenomena. *Icarus* **1995**, *114*, 130−138.
(29) Manning, H. L. K.; ten Kate, I. L.; Battel, S. J.; Mahaffy, P. R. Electric discharge in the Martian atmosphere, Paschen curves and implications for future missions. *Adv. Space Res.* **2010**, *46*, 1334−1340.
(30) Conti, V. J.; Williams, A. W. Ionization growth in carbon dioxide. *J. Phys. D: Appl. Phys.* **1975**, *8*, 2198−2207.
(31) Eden, H. F.; Vonnegut, B. Electrical Breakdown Caused by Dust Motion in Low-Pressure Atmospheres: Considerations for Mars. *Science* **1973**, *180*, 962−963.
(32) Lang, F.; Jošt, M.; Bundesmann, J.; Denker, A.; Albrecht, S.; Landi, G.; Neitzert, H.-C.; Rappich, J.; Nickel, N. H. Efficient minority carrier detrapping mediating the radiation hardness of triple-cation perovskite solar cells under proton irradiation. *Energy Environ. Sci.* **2019**, *12*, 1634−1647.
(33) Huang, K.; Yang, K.; Li, H.; Zheng, S.; Wang, J.; Guo, H.; Peng, Y.; Zhong, X.; Yang, J. γ-ray Radiation on Flexible Perovskite Solar Cells. *ACS Appl. Energy Mater.* **2020**, *3*, 7318−7324.
(34) Lorenz, R. D.; Martínez, G. M.; Spiga, A.; Vicente-Retortillo, A.; Newman, C. E.; Murdoch, N.; Forget, F.; Millour, E.; Pierron, T. Lander and rover histories of dust accumulation on and removal from solar arrays on Mars. *Planet. Space Sci.* **2021**, *207*, 105337.
(35) Wu, Z.; Ling, Z.; Zhang, J.; Fu, X.; Liu, C.; Xin, Y.; Li, B.; Qiao, L. A Mars Environment Chamber Coupled with Multiple In Situ Spectral Sensors for Mars Exploration. *Sensors* **2021**, *21*, 2519.
(36) Pan, T.; Zhou, W.; Wei, Q.; Peng, Z.; Wang, H.; Jiang, X.; Zang, Z.; Li, H.; Yu, D.; Zhou, Q.; Pan, M.; Zhou, W.; Ning, Z. Surface-Energy-Regulated Growth of α-Phase $Cs_{0.03}FA_{0.97}PbI_3$ for Highly Efficient and Stable Inverted Perovskite Solar Cells. *Adv. Mater.* **2023**, *35*, 2208522.
(37) Munguira, A.; Hueso, R.; Sánchez-Lavega, A.; de la Torre-Juarez, M.; Martínez, G. M.; Newman, C. E.; Sebastian, E.; Lepinette, A.; Vicente-Retortillo, A.; Chide, B.; Lemmon, M. T.; Bertrand, T.; Lorenz, R. D.; Banfield, D.; Gómez-Elvira, J.; Martín-Soler, J.; Navarro, S.; Pla-García, J.; Rodríguez-Manfredi, J. A.; Romeral, J.; Smith, M. D.; Torres, J. Near Surface Atmospheric Temperatures at Jezero From Mars 2020 MEDA Measurements. *J. Geophys. Res.: Planets* **2023**, *128*, No. e2022JE007559.
(38) Leovy, C. Weather and climate on Mars. *Nature* **2001**, *412*, 245−249.
(39) Miyazawa, Y.; Ikegami, M.; Chen, H.-W.; Ohshima, T.; Imaizumi, M.; Hirose, K.; Miyasaka, T. Tolerance of Perovskite Solar

https://doi.org/10.1021/acsomega.4c02887
ACS Omega 2024, 9, 25215−25222

Cell to High-Energy Particle Irradiations in Space Environment. *iScience* **2018**, *2*, 148−155.
(40) Chen, Y.; Tan, S.; Li, N.; Huang, B.; Niu, X.; Li, L.; Sun, M.; Zhang, Y.; Zhang, X.; Zhu, C.; Yang, N.; Zai, H.; Wu, Y.; Ma, S.; Bai, Y.; Chen, Q.; Xiao, F.; Sun, K.; Zhou, H. Self-Elimination of Intrinsic Defects Improves the Low-Temperature Performance of Perovskite Photovoltaics. *Joule* **2020**, *4*, 1961−1976.

https://doi.org/10.1021/acsomega.4c02887
ACS Omega 2024, 9, 25215−25222